

Preparation and optical characterization of Au/SiO₂ composite films with multilayer structure

H. B. Liao

Department of Physics, Hong Kong University of Science and Technology, Clear Water Bay, Kowloon, Hong Kong and Department of Physics, Beijing Normal University, Beijing, 100875, The People's Republic of China

Weijia Wen^{a)} and G. K. L. Wong

Department of Physics, Hong Kong University of Science and Technology, Clear Water Bay, Kowloon, Hong Kong

(Received 22 November 2002; accepted 21 January 2003)

An investigation of Au/SiO₂ composite multilayer films with a large third-order optical nonlinearity is reported in this article. Multilayer films containing Au nanoparticles with narrow size and shape distributions can be obtained by controlling the thickness of the Au layer, as well as the annealing temperature and time duration. It is found that the peak of surface plasmon resonance (SPR) of films with mean nanoparticle size of 30 nm is located at 2.35 eV with a width of 350 meV. The SPR peak of films containing larger or smaller particles red-shifts and broadens due to the particle size and shape effects. The third-order optical nonlinear susceptibility $\chi^{(3)}$ of these films has a maximum value of about 5.1×10^{-6} esu at 532 nm when the mean nanoparticle size is around 30 nm. We attribute the observed size dependence of $\chi^{(3)}$ to the competition between the enhancement of the local field factor and the skin-depth effect. © 2003 American Institute of Physics.

[DOI: 10.1063/1.1560569]

I. INTRODUCTION

Composite materials with dielectric matrix and metal nanoparticles (such as Au, Ag, and Cu) are attractive candidates for future photonic device applications due to their large third-order nonlinear susceptibility, $\chi^{(3)}$, and fast response time, which stems from the enhancement of the local field factor near the surface plasmon resonance (SPR).¹⁻³ In the last decade, a mass of research works focused on further improvement of the value of nonlinearity by changing matrix materials and increasing the concentration of metal particles to the percolation threshold.⁴⁻⁷ Also, various techniques of sample preparation were used to incorporate more metal particles into the substrate, such as ion implantation,⁶ sputtering^{4,5,7} and sol-gel.⁸ Usually, metal particles with a wide size distribution were randomly dispersed inside these materials. It was reported that the effective third-order nonlinear susceptibility in such materials were strongly influenced by the homogeneous dephasing time of the surface plasmon, which was related to the size, the shape, the surface structure, and the dielectric environment of the individual metal particles.^{9,10} Thus composite films containing a uniform distribution of particles with suitable size and shape might exhibit further enhanced third-order nonlinear susceptibility.

On the other hand, materials with a narrow distribution of particle size and shape are necessary for studying the size dependence of the optical properties in order to better understanding the origin of the enhancement of the nonlinearity in

such metal-dielectric composites. Although a few early studies involved the size dependence of the $\chi^{(3)}$, their samples were mostly fabricated with low metal concentration (with only a few percentages in volume fraction) and small particle size.^{7,11,12} Reference 11 reported that the real part of the $\chi^{(3)}$ in the Cu-doped Al₂O₃ was proportional to $1/d^3$ in the particle size range of less than 15 nm due to the quantum confinement effect, where d was the diameter of the Cu particles. But for Au particles, near the SPR peak, the imaginary part of $\chi^{(3)}$ was five times in value of the real part.¹³ That is, the contribution from the light absorption in the Au-doped composite film would dominate the enhancement of $\chi^{(3)}$ and thus may result in a different size dependence relationship.

In this article, we report our preparation of Au/SiO₂ composite films that are of multilayer structure with a narrowly distributed particle size and shape. The size dependence of the linear and nonlinear optical properties has also been characterized. For constant Au concentration of 26% atomic fraction, the effective $\chi^{(3)}$ of the samples with mean particle size around 30 nm is found to have a maximum value of 5.1×10^{-6} esu measured by degenerate four-wave mixing (DFWM) at 532 nm. The SPR peak redshifts and broadens for both smaller and larger Au particles due to the influence of the particle size and shape.

II. EXPERIMENT

The Au/SiO₂ multilayer films were prepared in a multi-target magnetron sputtering system (Denton SJ/24 LL) which was described in detail elsewhere.¹⁴ In this sputtering system, the Au (99.999%) and SiO₂ (99.99%) targets, which were 2 in. in diameter, were connected to two independent rf

^{a)} Author to whom correspondence should be addressed; electronic mail: phwen@ust.hk

power supplies. The Au layer and SiO₂ layer could be alternatively deposited onto the substrates at room temperature. The deposition rate of Au and SiO₂ were first calibrated by separately sputtering of Au and SiO₂ under the same deposition condition. The typical deposition rate of Au and SiO₂ used was about 0.06 nm and 0.04 nm per second, respectively. The heat treatment of the as-grown samples was carried out in a thermal furnace, in which the heating/cooling rate and the annealing duration could be automatically adjusted by setting the program parameters. The annealing temperature used in our experiments ranged from 850 to 1050 °C and the annealing time from 1 min to 10 h in order to obtain Au particles with different sizes.

X-ray photoelectron spectroscopy (XPS) and x-ray fluorescence spectroscopy (XRF) were used to measure the Au concentrations of the films deposited on fuse quartz and MgO substrate, respectively. The crystallinity of the Au particles was investigated by the x-ray diffraction (XRD) method (model: Philips PW1830). The mean size of Au particles could be estimated by measuring the full width at half maximum (FWHM) of the diffraction peaks and using the Scherrer's equation. Transmission electron microscopy (TEM) (model: Philips CM120) was applied to reveal the images of the cross-sectional microstructure of selected Au/SiO₂ composite films and the size-distribution was obtained by analyzing the individual Au particles in the TEM pictures.

The linear optical absorption spectra of the Au/SiO₂ films were measured by an ultraviolet-visible (UV)-VIS spectrophotometer (Perkin Elmer, lambda 20) in the range between 300 and 1000 nm. The third-order nonlinear susceptibility $\chi^{(3)}$ was measured at 532 nm using a Nd:YAG laser (*Q* switched and mode locked) and employing a standard backward DFWM scheme. The laser had a pulse duration of 70 ps, a repeat rate of 500 Hz, and a maximum peak power of about 6.5 MW/cm². A high sensitivity photodiode and a lock-in amplifier were used to detect the nonlinear signals. The value of the effective $\chi^{(3)}$ was measured relative to CS₂, a reference medium which has a $\chi^{(3)} = 2 \times 10^{-12}$ esu in the picosecond time scale, by using the following equation:

$$\chi^{(3)} = \chi_{CS_2}^{(3)} \sqrt{\frac{I_s}{I_{CS_2}}} \frac{n_s^2}{n_{CS_2}^2} \frac{L_{CS_2}}{L_s} \frac{1}{(1-T)\sqrt{T}} \ln \frac{1}{T}, \quad (1)$$

where I_s and I_{CS_2} are the intensity of the conjugate signal, n_s and n_{CS_2} , the respective refractive indices, L_s and L_{CS_2} the thickness of the Au/SiO₂ composite films and the CS₂, respectively, and T is the transmissivity of the Au/SiO₂ films at a given laser wavelength.

III. RESULTS AND DISCUSSIONS

The Au concentration of the samples reported in this article, before or after thermal annealing, is about 26% ± 1% in atomic fraction given by the XPS and XRF methods. After annealing, the Au/SiO₂ composite films are of beautiful ruby-like colors instead of dark brown before annealing due to the formation of the Au particles.

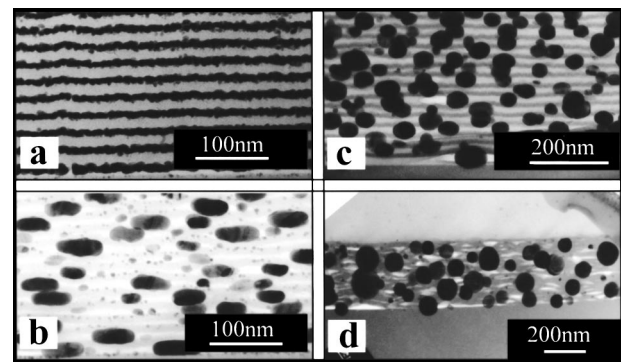


FIG. 1. Selected cross-section TEM pictures of the Au/SiO₂ multilayer films with Au concentration of about 26% in atom fraction: (a) as-deposited film; films annealed at: (b) 950 °C for 1 min; (c) 950 °C for 5 h; (d) 1050 °C for 5 h.

Selected cross-sectional TEM pictures are shown in Fig. 1, where the thickness of Au layers of these samples is the same (about 4 nm). It is obvious that the as-grown film [Fig. 1(a)] has a well-controlled Au/SiO₂ multilayer structure with a period of about 25 nm and its morphology remains almost the same for the samples annealed, even up to 950 °C for 1 min [Fig. 1(b)] and 5 h [Fig. 1(c)]. From Fig. 1, we can see that the Au particles are very small and connect with each other forming a uniform film before annealing [Fig. 1(a)]. However, as can be seen in Fig. 1(b), during annealing, the Au particles aggregate much faster in the direction parallel to the film surface (about 35 nm in dimension) than that in the direction perpendicular (about 16 nm in dimension) to it. This is due to the confinement effect of the SiO₂ layers, which sandwich the Au layers. As a result, Au particles with disk-like shape are usually observed. With longer annealing time [Fig. 1(c)], most of the particles grow to be ellipsoid in shape and about 40 nm in size. However, when the sample is annealed at 1050 °C for 5 h, the multilayer structure is destroyed and the film shrinks down to contact each other and the film thickness is reduced to only half of that of the as-grown films. In this case, large spherical Au particles, with a mean size of 80 nm, are formed through the coalescence of Au particles from different layers. We also find that the multilayer structure smears out when the Au layer becomes thinner (less than 3 nm), in which case, the Au particles are spherical in shape and only several nanometers in size even after being annealed at 950 °C for 10 h (TEM pictures not shown here), and this morphology is very similar to that reported in Ref. 7.

The TEM images suggest that our samples have a fairly uniform distribution both in Au particle shape and size. A micrograph field including more than 250 particles was randomly selected to analyze the size distribution of the Au particles. The distribution of the particle size parallel to the SiO₂ layer is plotted in Fig. 2(a) for the sample of Fig. 1(c), which has a mean value of 48 nm with a standard deviation of 27%. Figure 2(b) shows the distribution of the particle size in the direction perpendicular to the SiO₂ layer, which has a smaller mean size (about 39 nm) and a narrower distribution (with a standard deviation about 25%) as a result of the confinement effect of the SiO₂ layers. The dashed lines in Fig. 2

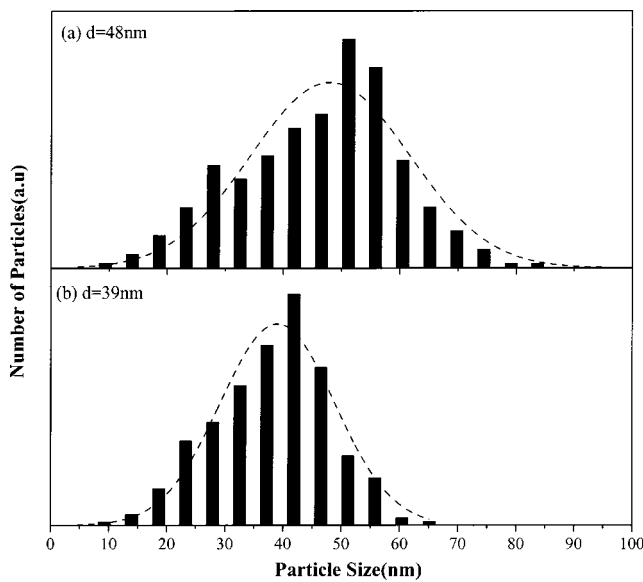


FIG. 2. The statistic size distribution of the Au/SiO₂ film used in Fig. 1(c). The dash line is the Gaussian fitting curve. Direction of the particle size: (a) parallel to the film surface; and (b) perpendicular to the film surface.

represent the Gaussian fitting curves. Given the same thickness of the Au layer and SiO₂, as well as the annealing temperature and time duration, the films obtained in different runs give essentially the same distribution. By changing these parameters, films with different distribution of size and shape of Au particles can be consistently obtained.

Two typical UV-VIS spectra of the as-grown and annealed samples are shown in the insets of Fig. 3. For the as-grown films (curve a), the SPR peak is located at the wavelength of 616 nm with a large FWHM value and a strong absorption in the near IR range. After thermal annealing (curve b), a distinguished SPR peak emerges and its FWHM of the SPR peak is much narrower than that prepared

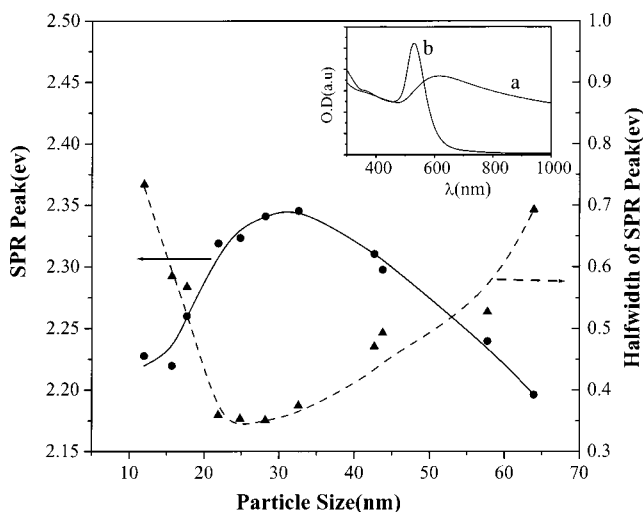


FIG. 3. Size dependence of the SPR peak and its FWHM of the Au/SiO₂ multilayer films. The Au concentration in all those samples is 26% in atomic fraction. The inset is the selected optical spectra: (a) as-grown film; and (b) annealed film.

by cosputtering method.⁴ Also, the film becomes almost transparent at wavelength range between 700 and 1000 nm.

In order to better understand the relation between the particle size and the SPR peak position as well as the FWHM, several samples were prepared with the same Au and SiO₂ layer thicknesses but annealed at different temperatures for different duration. The results are plotted in Fig. 3 as a function of the mean diameters of Au particle measured by XRD method. We find that the SPR peak position and their FWHM do not monotonically change with the increase of the particle size, which is the usual case reported in the literature.^{10,12} As seen in Fig. 3, the sample with a mean size around 30 nm has the bluest and narrowest SPR peak, located at 2.35 eV (about 530 nm in wavelength) with a FWHM of about 350 meV. But the SPR peak redshifts and broadens when the mean diameter of the Au particles becomes smaller or larger. It is easy to understand the redshift effect for the large particles, which is attributed to the surface retardation effect.¹⁰ The redshift and broadening observed in our small mean-diameter Au particle films may be due to other effects. We find that the SPR peak of films containing small (several nanometers in diameter) spherical Au particles (obtained by annealing the multilayer structure with the thin Au layer), is at around 2.35 eV with a very narrow FWHM (about 0.376 eV), which is almost the same as that observed in the sample with a particle size of 30 nm mentioned above. This suggests that the observed anomalous redshift and broadening is likely due to anisotropy in the particle shape. Upon deformation into ellipsoidal shape, the SPR peak of Ag spherical particles has been observed to split into two spectrally separate SPR peaks that can be excited with light polarized parallel to the long and short axis, respectively.¹⁵ Since the ellipsoidal particles in our sample are not expected to be uniformly oriented, the measured SPR peak can appear broadened and redshifted, as the long axis SPR is strongly redshifted as compared to the small blueshift of the short axis SPR.

The calculated values of the third-order susceptibility $\chi^{(3)}$ are plotted in Fig. 4 as a function of the size of the Au particles in the annealed Au/SiO₂ multilayer films. It should be mentioned here that some of the samples shown in Fig. 3 were damaged during the measurement of $\chi^{(3)}$ when they were annealed at a lower temperature or for a shorter time. This is due to the very strong intense laser radiation on the sample causing thermal damage during the DFWM measurement. All of the samples used here are found to have ellipsoid Au particles and their SPR peaks are very close to the laser wavelength. As shown in Fig. 4, the value of $\chi^{(3)}$ is only about 9×10^{-7} esu at the particle size of 16 nm, while the $\chi^{(3)}$ increases rapidly and reaches a value of 5.1×10^{-6} esu when the particle size is around 30 nm. However, with further increase in particle size, $\chi^{(3)}$ decreases and remains around 2.3×10^{-6} esu. For those with particle size being larger than 100 nm, the strong light scattering causes a weakening of the conjugate signals and makes it almost immeasurable.

It is well known that the enhancement of $\chi^{(3)}$ in the metal/dielectric composite is strongly dependent on the non-linearity of the metal particle itself and on the so-called local

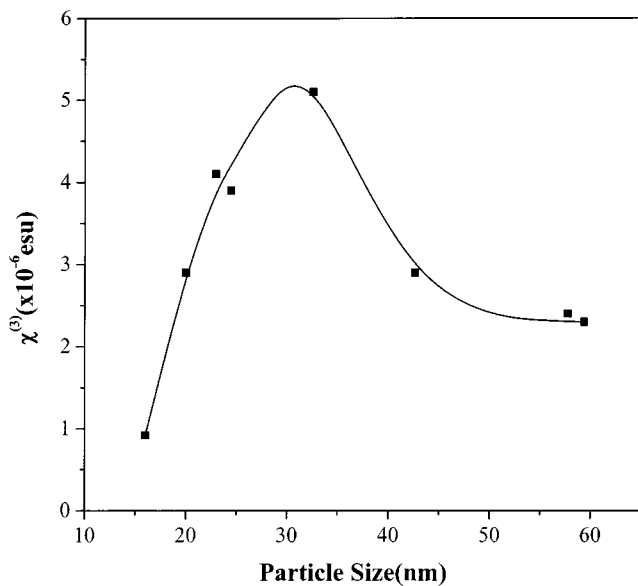


FIG. 4. Size dependence of the third-order optical nonlinear susceptibility $\chi^{(3)}$ measured at laser wavelength of 532 nm with a pulse duration of 70 ps.

field factor $f=3\epsilon_d/(\epsilon_m+2\epsilon_d)$, where ϵ_m and ϵ_d are the dielectric constant of the metal and the dielectric matrix, respectively. The $\chi^{(3)}$ of Au particles can be decomposed into three parts: the intraband transition, the interband transition, and the hot electron contribution. The first term is size dependent ($\propto 1/d^3$) and the other two are not. However, the contribution of the hot electrons is about 1 order larger than that of the interband term and about 3 orders larger than that of the intraband term for Au particles of 5 nm.³ That is, the $\chi^{(3)}$ of the Au particles can be regarded as a constant in our samples and is mainly attributed to the hot electrons. Therefore, the local field factor is assumed to play an important role on the size dependence of the $\chi^{(3)}$ shown in Fig. 4.

Near resonance, the local field factor can be written as $f=3\epsilon_d/i\epsilon_{m2}$, where ϵ_{m2} is the imaginary part of the metal dielectric constant, which decreases with increasing particle size.¹⁰ So, the larger the particle size, the larger the local field factor, and the bigger the value of $\chi^{(3)}$. With the increasing size of Au particles, the dielectric constant approaches that of the bulk gold. As a result, the values of f and $\chi^{(3)}$ gradually become constant. On the other hand, the attenuation of the electric field inside the particles and the light scattered outside the particles must be considered for the large particles. This will cut down the value of $\chi^{(3)}$ because in this case only the surface layer of the particles responds to the outside electric field. This is equivalent to a decrease in metal concen-

tration. Therefore, it is the competition between these two aspects that brings about the size dependence of $\chi^{(3)}$ as displayed in Fig. 4.

IV. CONCLUSIONS

We have prepared a set of Au/SiO₂ multilayer films with a high Au concentration by magnetron sputtering method, where uniform distribution both on size and shape of metal nanoparticles can be obtained. It is found that the peak of surface plasmon resonance of the film with a mean size of 30 nm is located at 2.35 eV with a width of 350 meV, while a redshift and broadening of the SPR peak occur in films containing larger and smaller particles due to the particle size and shape effect. The third-order nonlinear susceptibility $\chi^{(3)}$ of the composites measured by DFWM is found to also have a maximum value around 30 nm. We attribute the size dependence of the $\chi^{(3)}$ to the competition between the enhancement of the local field factor and the attenuation of the electric field inside the Au particles.

ACKNOWLEDGMENTS

This work was supported by RGC Hong Kong through Grant Nos. N_HKUST025/00 and HKUST6153/00P.

- ¹*The Principle of Nonlinear Optics*, edited by Y. R. Shen (Wiley, New York, 1984).
- ²D. Ricard, P. Roussignol, and C. Flytzanis, *Opt. Lett.* **10**, 511 (1985).
- ³C. Flytzanis, F. Hache, M. C. Klein, D. Ricard, and P. Rousignol, in *Progress in Optics XXIX*, edited by E. Wolf (Elsevier Science, North-Holland, Amsterdam, 1991), p. 321.
- ⁴H. B. Liao, R. F. Xiao, J. S. Fu, P. Yu, G. K. L. Wong, and P. Sheng, *Appl. Phys. Lett.* **70**, 1 (1997).
- ⁵H. B. Liao, R. F. Xiao, H. Wong, K. S. Wong, and G. K. L. Wong, *Appl. Phys. Lett.* **72**, 1817 (1998).
- ⁶R. H. Magruder III, L. Yang, R. F. Haglund, C. W. White, L. Yang, R. Dorsinville, and R. R. Alfano, *Appl. Phys. Lett.* **62**, 1730 (1993).
- ⁷I. Tanahashi, Y. Manabe, T. Tohda, S. Sasaki, and A. Nakamura, *J. Appl. Phys.* **79**, 1224 (1996).
- ⁸S. Ogawa, Y. Hayashi, N. Kobayashi, T. Tokizaki, and A. Nakanura, *Jpn. J. Appl. Phys., Part 2* **33**, L331 (1994).
- ⁹T. Klar, M. Perner, S. Grosse, G. von Plessen, W. Spirkle, and J. Feldmann, *Phys. Rev. Lett.* **80**, 4249 (1998).
- ¹⁰*Optical Properties of the Metal Clusters*, edited by U. Kreibig and M. Vollmer (Springer, Berlin, 1995).
- ¹¹J. M. Ballesteros, J. Solis, R. Serna, and C. N. Afonso, *Appl. Phys. Lett.* **74**, 2791 (1999).
- ¹²G. Ma, W. Sun, S. H. Tang, H. Zhang, Z. Shen, and S. Qian, *Opt. Lett.* **27**, 1043 (2002).
- ¹³D. D. Smith, Y. Yoon, R. W. Boyd, J. K. Campbell, L. A. Baker, R. M. Crooks, and M. George, *J. Appl. Phys.* **86**, 6200 (1999).
- ¹⁴*Handbook of Nonlinear Optics*, edited by Richard L. Sutherland (Marcel Dekker, Inc. New York, 1996).
- ¹⁵R. Borek, K. J. Berg, and G. Berg, *Glass Sci. Technol. (Amsterdam)* **71**, 352 (1998).